Geometry-Information-Aided Efficient Radial Velocity Estimation for Moving Target Imaging and Location Based on Radon Transform

Xuepan Zhang, Guisheng Liao, *Member, IEEE*, Shengqi Zhu, *Member, IEEE*, Cao Zeng, *Member, IEEE*, and Yuxiang Shu

***Abstract*—Real-time radial velocity estimation is a key challenge for moving target imaging and location in current single-antenna synthetic aperture radar (SAR)-ground moving target indication systems. Since the conventional methods suffer from ambiguity, complexity realization, or heavy computation load for fast moving target motion estimation, this paper emphasizes the estimation efficiency by simple realization. An efficient Radon transform (RT) estimation is proposed to estimate the radial velocity of fast moving target by utilizing the geometry information, and much more geometry information is exploited to realize clutter cancellation, noise cancellation, and estimation error minimizing in the RT domain, which is not proposed by the others. With only two to four angles used to calculate rather than search for the radial velocity of moving targets, the proposed methods simplify the conventional range and angle (2-D) searching procedure into several time range (1-D) searching procedure efficiently. The theoretical and experimental analysis provides qualitative and quantitative evaluations into the effectiveness of the proposed methods. In the single-antenna SAR system, the proposed methods can estimate the radial velocity of fast moving target efficiently and accurately in high signal to clutter plus noise ratio scenarios.**

***Index Terms*—Efficient estimation, geometry information, radial velocity estimation, Radon transform (RT), synthetic aperture radar (SAR)-ground moving target indication (GMTI).**

I. Introduction

SYNTHETIC aperture radar (SAR)-ground moving target indication (GMTI) is widely used in civilian and military areas with increasing requirements [1]–[5]. Moving target imaging and localization in the SAR image are very meaningful for recognizing and tracking targets [6], [7]. Due to the radial velocity, the moving target is not only induced by severe range walk [8], [9] but also azimuthally displaced in the final SAR image [10], [11], which is not beneficial for moving target imaging and localization. Moreover, mismatch between the estimated radial velocity and its real value increases the burden on recognition and degrades the localization and tracking performance decisively. Herein, as the essential prerequisite parameter, the radial velocity of moving targets should be estimated accurately. However, the existing radial velocity estimation methods described afterward suffer from ambiguity, complexity realization, or heavy computation load. Consequently, unambiguous and efficient radial velocity estimation is a key challenge for the current low complexity realization SAR systems, particularly for single-channel SAR systems. In this paper, by utilizing the single-channel SAR, we focus on unambiguously and efficiently estimating the radial velocities of fast moving targets which move one range resolution at least in the synthetic aperture time.

Skilled at clutter suppression, multichannel SAR is routinely used to estimate the radial velocity of moving targets. It is well known that the radial velocity can be estimated directly from the interferometric phase obtained by the along-track interferometry (ATI) [12], [13]. However, the ATI-based radial velocity estimation methods suffer from phase wrapping. Conventionally, multifrequency antenna array SAR [14] or velocity SAR [15] is adopted to increase the estimated maximum unambiguous radial velocity. However, these burden the system realization seriously. On the other hand, characterized by much simpler and cheaper realization, the single-channel SAR-GMTI system which is easy to be deployed in satellites [16] is studied with continuing interest. For single-channel SAR systems, the Doppler shift induced by the radial velocity can be used to estimate the radial velocity. Nevertheless, ambiguity occurs when the Doppler shift exceeds half of the pulse repetition frequency (PRF), and thereby, increasing PRF [17] and multiple PRFs [18], [19] are used to release the limitation. However, increasing PRF not only shortens the unambiguous range swath but also burdens on data memorizing, and multiple PRFs require much more complex imaging algorithm, which should not be encouraged and generalized in modern agile and efficient SAR systems [6].

Given the disadvantages of the aforementioned phase-based estimation methods, some authors propose the ambiguity-free amplitude-based methods to estimate the radial velocity unambiguously. Range cell migration correction is used to find the matched radial velocity by searching any possible values. In addition, the skewed trajectory of moving targets (i.e., the

Manuscript received December 14, 2013; revised April 25, 2014; accepted June 19, 2014. This work was supported by the National Basic Research Program of China under Grant 2010CB731903, by the Aeronautic Fund under Grant 20121081004, by the National Nature Science Foundation of China under Grants 61101249, 61231017, and 61101243, and by the Graduate Innovation Foundation of Xidian University under Grant JB142001-11.

X. Zhang, G. Liao, S. Zhu, and C. Zeng are with the National Laboratory of Radar Signal Processing, Xidian University, Xi'an 710071, China (e-mail: xpzhang7@163.com; liaogs@xidian.edu.cn).

Y. Shu is with No.38 Research Institute, China Electronics Technology Group Corporation, Hefei 230088, China (e-mail: shuyuxiang723@163.com).

Color versions of one or more of the figures in this paper are available online at http://ieeexplore.ieee.org.

Digital Object Identifier 10.1109/TGRS.2014.2334322

range walk) due to the radial velocity in the range compression domain can also be utilized to estimate the radial velocity. Capable of estimating the skewed angle of straight line in the 2-D plane, Radon transform (RT) is often used to estimate the range walk angle of the moving target, and then, the radial velocity can be obtained [20]. In the conventional RT estimation (CRTE) method, angles and ranges are searched in the 2-D plane to find the best matched angle. However, the 2-D searching operation brings heavy computation load. Moreover, it is noteworthy that the searching step size of angles influences not only the computation complexity but also the estimation accuracy [8]. Therefore, the tradeoff between the estimation accuracy and the computation complexity should be handled in the CRTE method. As is known, both of the heavy computation load and the tradeoff restrict the application of the CRTE method in practice, especially for the real-time estimation. In order to remedy the disadvantages of the CRTE method, multiple angle searching steps, instead of a single step, are used to find the best matched angle: A larger step is used to find the approximate interval of the best matched angle with low computation complexity, and then, a smaller step is used to search a much more accurate range walk angle in the obtained interval for radial velocity estimation. Moreover, the radial velocity can be expressed by its baseband velocity v_{rb} and the ambiguity number M as $v_r = v_{rb} + M \cdot v_{r\max}$, where $v_{r\max}$ is the estimated maximum unambiguous radial velocity. Since the baseband velocity is proportional to the baseband Doppler centroid, which can be estimated by [21], only several possible ambiguity numbers are used to search for the matched ambiguity number [22]–[24], and then, the radial velocity can be obtained.

Different from the searching-based estimation methods, an efficient RT estimation (ERTE) method is proposed to reduce the heavy computation load. By utilizing the geometry information in the RT domain, the best matched range walk angle is calculated by only two angles rather than by searching all possible angles. Therefore, the proposed method simplifies the original 2-D searching operation into only two times 1-D searching operation. Therefore, the heavy computation load is reduced effectively, and the tradeoff between the computation complexity and the estimation accuracy is avoided simultaneously. Real circumstances with clutter, noise, and estimation error due to angle selection are analyzed, and the corresponding robust methods are also proposed by exploiting the geometry information further.

This paper is organized as follows. Section II reviews the RT-based radial velocity estimation for moving targets. Section III describes the ERTE method in the absence of both clutter and noise. Section IV analyzes the real circumstance with clutter, noise, and estimation error, and the corresponding robust methods including clutter suppression RT estimation (CSRTE), noise background RT estimation (NBRTE), and angle learning RT estimation (ALRTE) are presented, respectively; afterward, a unified robust RT estimation (URRTE) is given by incorporating the three robust methods together. Section V shows the simulation and real data process to demonstrate the validity of the proposed methods. Section VI concludes this paper and develops further research.

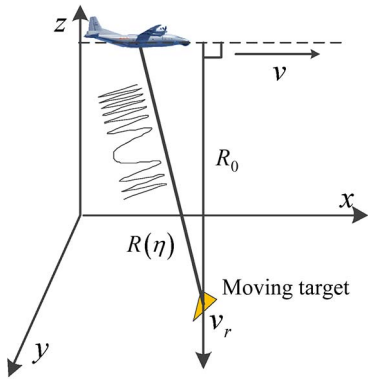

Fig. 1. Geometry of a moving target in the single-antenna SAR system.

II. Signal Model

The ideal circumstance without clutter and noise is analyzed in this section, while the clutter and noise background would be discussed in Section IV. A typical side-looking single-antenna SAR configuration with a ground moving target is shown in Fig. 1. During the synthetic aperture time T_a, the SAR platform flies with a constant velocity v, and the moving target moves with a constant radial velocity v_r, where the other motion parameters of the moving target are ignored. The instantaneous slant range $R(\eta)$ from the moving target to the SAR platform can be obtained from the geometry, which can be expressed by the following second-order approximation in the Taylor expansion at $\eta = 0$

$$R(\eta) \approx R_0 + v_r\eta + \frac{v^2}{2R_0}\eta^2 \tag{1}$$

where η denotes the slow time in azimuth and R_0 is the nearest slant range from the moving target to the SAR track. After range compression and range curvature correction [25], the signal of the moving target can be rewritten as

$$s(\tau,\eta) = \sigma_s A \cdot \operatorname{sinc}\left[B_r\left(\tau - 2(R_0 + v_r\eta)/c\right)\right] \cdot \operatorname{rect}\left[\frac{\eta}{T_a}\right] \exp\left(-j4\pi f_c R(\eta)/c\right) \tag{2}$$

where σ_s is the complex reflection coefficient of the moving target, A is the range compression gain, B_r is the bandwidth of the transmitted linear frequency modulated signal, τ is the fast time in range, f_c denotes the carrier frequency, and c is the speed of light.

The result of (2) is shown as Fig. 2(b), where the range walk due to the radial velocity occurs. It is well known that the range walk is not conducive to moving target imaging, and the radial velocity of the moving target should be estimated to correct the range walk. It should be pointed out that the radial velocity of the moving target is contained in the amplitude information of (2), so the amplitude information is used to estimate the radial velocity. For the amplitude-based estimation method, the moving targets to be estimated should move across one range resolution ρ_r at least in the synthetic aperture time (i.e.,$|v_r|T_a \geq \rho_r$), so the minimum estimated radial velocity can be given by the following mathematical form:

$$|v_{r,\min}| = \frac{\rho_r}{T_a}. \tag{3}$$

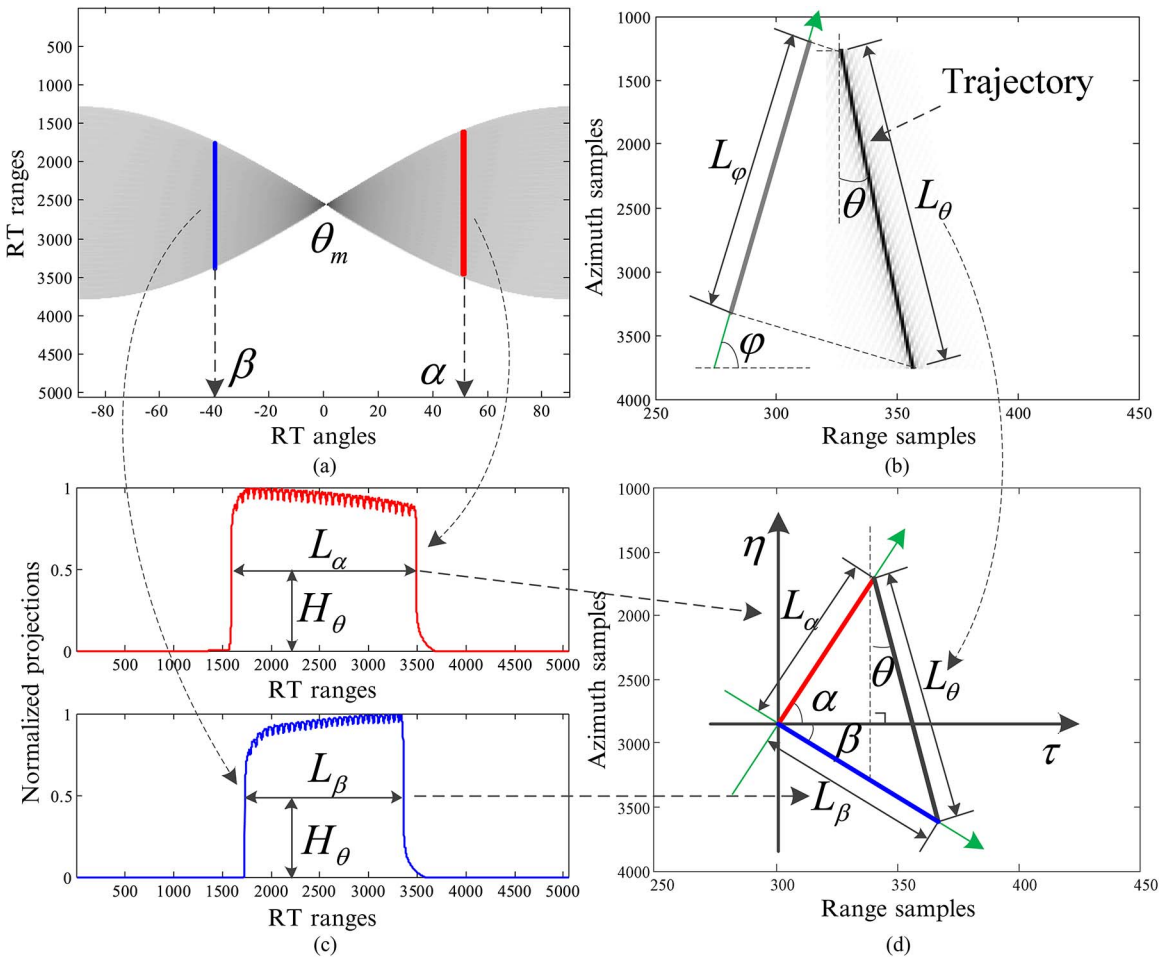

Fig. 2. Sketch of the ERTE method. (a) α- and β-RTs of moving targets. (b) Range compression result of moving targets. (c) Normalized projections of α- and β-RTs. (d) Geometric relationship between the LNPs and the range walk angle of moving targets.

As shown in Fig. 2(b), the range walk angle of the moving target is set as θ, and the relationship between the range walk angle and the radial velocity v_r can be expressed as

$$v_r = c \cdot \tan\theta \cdot f_{sa}/2f_{sr} \tag{4}$$

where f_{sa} and f_{sr} are the PRF in azimuth and the sampling frequency in range. Capable of angle estimation in the 2-D plane, RT can be defined as [26]

$$S_R(\rho,\varphi) = \int_{-\infty}^{+\infty}\int_{-\infty}^{+\infty} |s(x,y)|\,\delta(\rho - x\cos\varphi - y\sin\varphi)\,dx\,dy \tag{5}$$

where $s(x,y)$ denotes the signal of the moving target located at coordinates of (x,y), $|\bullet|$ is the absolute operation, $\delta(\cdot)$ is the impulse function, and $S_R(\rho,\varphi)$ is the φ-RT with range ρ and angle φ. As shown in Fig. 2(a), the CRTE method can be summarized as [20]: All RTs of $|s(x,y)|$ are performed first by all possible angles, and the angle corresponding to the peak value of the RT results is obtained as the best matched angle θ_m; afterward, the radial velocity of the moving target can be calculated via

$$\hat{v}_{r,\mathrm{CRTE}} = c \cdot \tan(\theta_m) \cdot f_{sa}/2f_{sr}. \tag{6}$$

Combining (3) with (6), we can obtain the effective scope of the estimated range walk angles by the RT-based estimation method

$$|c \cdot \tan\theta \cdot f_{sa}/2f_{sr}| > \frac{\rho_r}{T_a} \Rightarrow |\tan\theta|^{\mathrm{RT}}_{\min} = \frac{f_{sr}}{B_r f_{sa} T_a} \tag{7}$$

where $|\tan\theta|^{\mathrm{RT}}_{\min}$ is the tangent value of the minimum estimated range walk angle.

The principle of the CRTE method is simple; nevertheless, the angle and range searching procedure brings heavy computation load. Moreover, the angle searching procedure brings the tradeoff between estimation accuracy and computation complexity to CRTE [27], which would restrict the application of CRTE in practice. Thus, it is significant to exploit much more ERTE, especially for real-time estimation requirements.

III. ERTE Method

Motivated by relieving the restrictions of the CRTE method, we propose an ERTE method to calculate rather than search the best matched range walk angle of the moving target. Through exploiting the geometry information, the proposed ERTE method realizes radial velocity estimation by utilizing only two angles, which simplifies the original 2-D searching operation into two 1-D searching operations.

A. Basic Principle of the ERTE Method

In the range compression domain, the trajectory of the moving target with range walk angle θ is shown in Fig. 2(b). The length of the normalized trajectory measured by a normalized threshold H_θ can be set as L_θ. Reanalyzing the RT of (5), we can find that the nature of φ-RT can be regarded as the projection of the trajectory on angle φ. In the φ-RT domain, the length of the normalized projection (LNP) of the φ-RT result can be measured as L_φ by the same normalized threshold H_θ. Then, we can get the following geometry relationship

$$L_\theta \left|\cos\left(\theta + (90^\circ - \varphi)\right)\right| = L_\varphi. \tag{8}$$

Given (8) and the conservation of energy law, the moving target energy increases, and the LNP L_φ shortens as $|\theta + (90^\circ - \varphi)|$ approaches to 90°, as shown in Fig. 2(a).

If L_θ and L_φ are foreknowledge or easy to be measured, we can calculate θ by (8) with only one time range (1-D) searching operation. However, the length of the skewed trajectory L_θ is hard to be measured in the 2-D plane. Therefore, the α- and β-RTs are used, as shown in Fig. 2(a), to cancel the term of L_θ in (8). In Fig. 2(c), the LNPs of the two RTs are measured as L_α and L_β by H_θ, where H_θ is precognition assumedly, and the threshold selection would be analyzed in the next section.

According to the projection nature of the RT as (8), we can get the following geometry relationship among the RT angles, LNPs, and range walk angle, which is also shown in Fig. 2(d):

$$L_\theta \sin(\alpha - \theta) = L_\alpha \tag{9}$$

$$L_\theta \sin(\theta - \beta) = L_\beta \tag{10}$$

where $0^\circ < \alpha - \theta < 180^\circ$ and $0^\circ < \theta - \beta < 180^\circ$ are assumed to remove the absolute operation in (8). Moreover, the assumption is supported by the fact that the radial velocity of the ground moving target is limited. For instance, keeping in mind (4), the range walk angle of moving targets can be set as being in the interval of $[-5^\circ, 5^\circ]$, and the corresponding radial velocity scope can be calculated by (4) as [−218.7 m/s, 218.7 m/s], which is satisfactory for most ground moving targets. Therefore, the range of α and β can be determined in the range of $5^\circ < \alpha < 175^\circ$ and $-5^\circ > \beta > -175^\circ$ to keep (9) and (10) hold, respectively.

Division between (9) and (10) is done to cancel the L_θ term, and then, the estimation of $\tan\theta$ can be obtained as

$$\tan\hat{\theta} = \frac{L_\beta \sin\alpha + L_\alpha \sin\beta}{L_\beta \cos\alpha + L_\alpha \cos\beta}. \tag{11}$$

According to (4) and (11), the radial velocity of the moving target can be calculated via

$$\hat{v}_{r,\mathrm{ERTE}} = \frac{c f_{sa}}{2 f_{sr}} \frac{L_\beta \sin\alpha + L_\alpha \sin\beta}{L_\beta \cos\alpha + L_\alpha \cos\beta}. \tag{12}$$

The principle of the proposed ERTE method has been presented over. By utilizing only two angles, the ERTE method can calculate the radial velocity of the moving target, which sufficiently simplifies the original 2-D searching operation into two times 1-D searching operation. Furthermore, the tradeoff between the computation complexity and the estimation accuracy can also be avoided because the estimation procedure is independent of the angle searching operation.

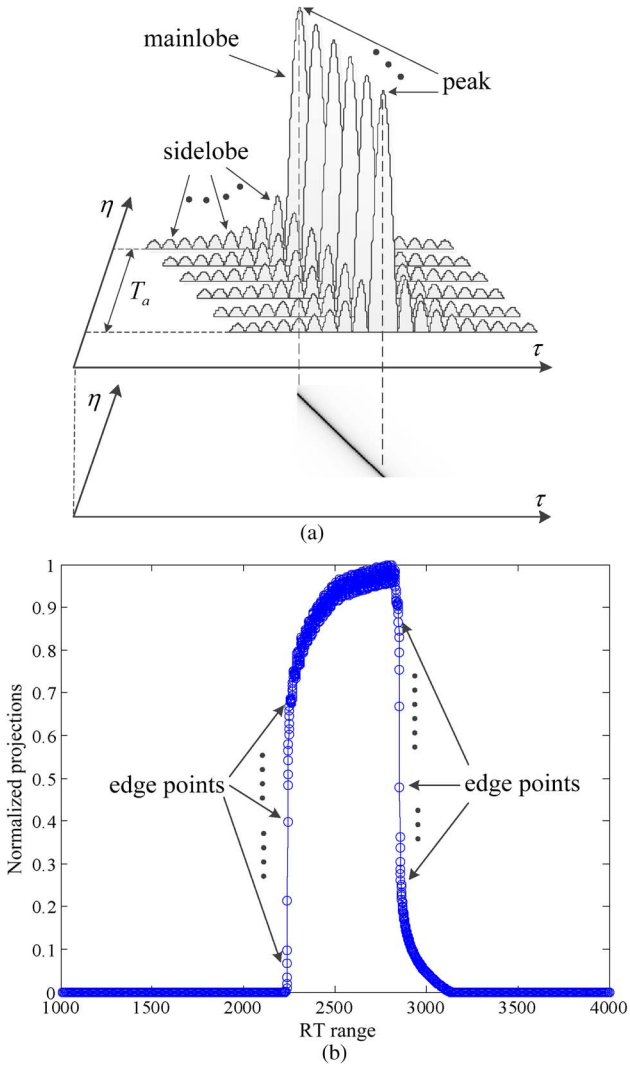

Fig. 3. Results without preprocessing. (a) Sinc function of the moving target trajectory. (b) Normalized projections of the φ-RT.

B. Threshold Selection Analysis

Reanalyzing the ERTE result of (12), we can find that only the measured LNPs (L_α and L_β) theoretically influence the estimation accuracy of the radial velocity, since the other parameters are foreknowledge. As aforementioned, the LNPs are measured by the normalized threshold H_θ. Without any processing, different normalized thresholds may result in different LNPs and therewith different radial velocity estimations. Thus, it is significant for accurate radial velocity estimation to analyze the normalized threshold selection. The normalized projection of the arbitrary φ-RT result is shown as Fig. 3(b).

It is reluctant to note that there are too many points on the edges, which burdens the threshold selection on accurate estimation. In other words, when the edges are gradually changing, different thresholds would lead to different LNPs and different radial velocity estimations. In this section, we mainly analyze the reason for the gradually changing edges, and a mainlobe

selection preprocessing is presented to release the burden of accurate estimation on threshold selection.

1) Burden on Accurate Estimation Due to Threshold Selection: First, the reason for the gradually changing edges is analyzed. As expressed in the range compression results of (2), the radial velocity regarding the moving target is contained in the sinc function.

Since the amplitude of the sinc function is used for the RT-based method to estimate the radial velocity, so the mainlobe (especially the peak value) of the sinc function contributes most to energy concentration in the φ-RT domain, while the sidelobe not only contributes less but also causes the gradually changing edges. Moreover, compared with the estimation using the peak value only, the estimation utilizing the mainlobe would be much more robust to the limit resolution of the SAR system. Therefore, the mainlobe rather than the peak value should be reserved to sharpen the edges of the RT projection.

2) Preprocessing Operation to Release the Burden of Threshold Selection: After the aforementioned theoretical analysis, a preprocessing is used to remove the sidelobe but reserve the mainlobe of the sinc function. The preprocessing operation can be described as follows: The peak value of each azimuth bin can be obtained first, the 3-dB value symmetry about the peak value can be confirmed, and then, the values beyond the range bins of the 3-dB values are set as zero. After the preprocessing in the range compression domain, the trajectory of the moving target and its φ-RT normalized projection are shown as Fig. 4(a) and (b), respectively. It is interesting to see from Fig. 4(b) that the edges of the normalized φ-RT result are sharp enough with only one point in each edge. Consequently, different normalized thresholds would result in almost the same LNPs and, therewith, the same radial velocity estimation. However, whether the estimation is accurate or not should be validated, which would be given in the next section.

3) Effect on the Estimation Accuracy by Preprocessing Operation: Since the 3-dB mainlobe is used to estimate the radial velocity, the thresholds around 0.5 should be focused. By utilizing different thresholds, the ERTE with preprocessing is compared with that without preprocessing, and the comparison results are shown in Fig. 5.

For the ERTE without preprocessing, the estimation accuracy obviously varies with the thresholds, while for that with preprocessing, the estimated results almost keep the same along with different thresholds. Most importantly, it is noteworthy that the estimation results with preprocessing are much more accurate than that without preprocessing. In a word, the simulation results validate that the preprocessing releases the burden of radial velocity estimation on threshold selection and, furthermore, improves the estimation accuracy. Therefore, the preprocessing is effective for the proposed ERTE method to accurately estimate the radial velocity.

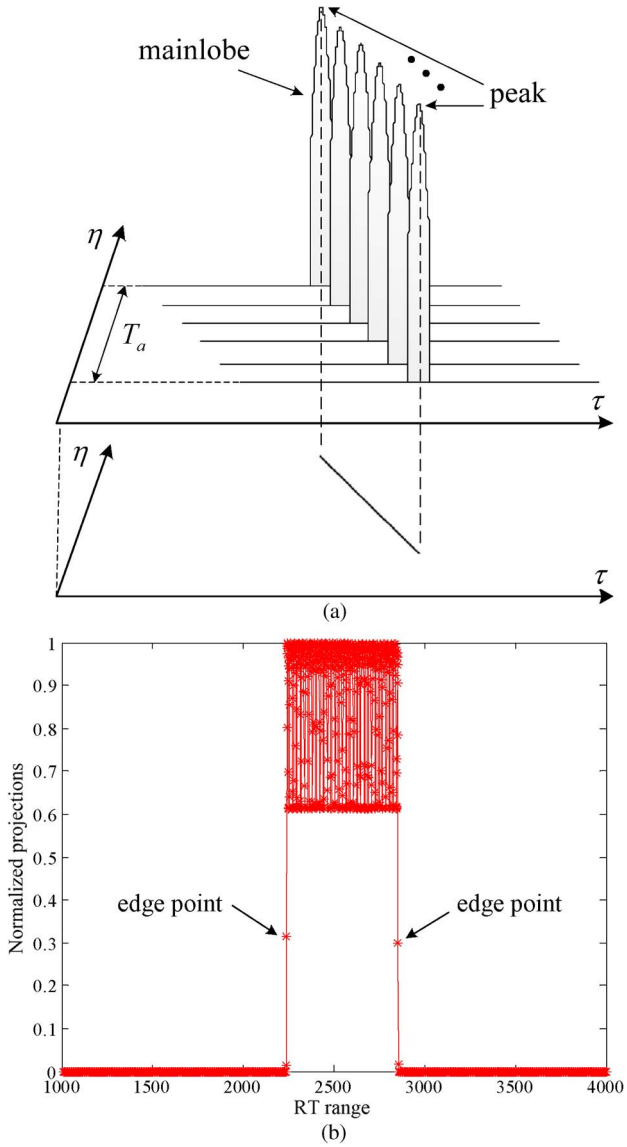

Fig. 4. Results with preprocessing. (a) Sinc function of the moving target trajectory. (b) Normalized projections of the φ-RT.

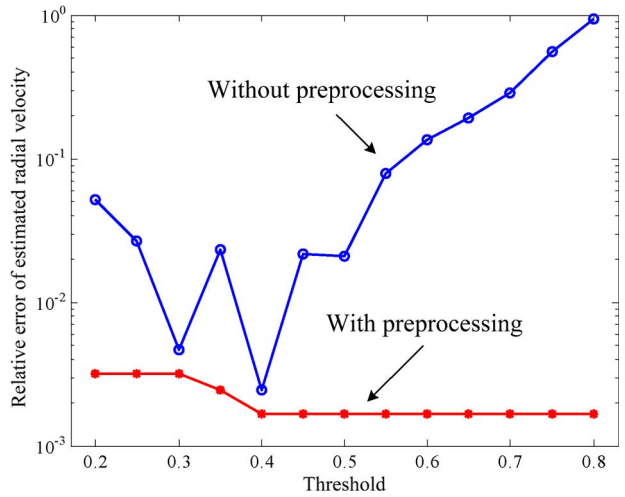

Fig. 5. Comparison between the estimations with and without preprocessing.

IV. Further Discussion of the Proposed Method

Real circumstance with clutter, noise, or estimation error due to angle selection would disturb the LNP measurement, which degrades the radial velocity estimation accuracy. In this section, the application of the ERTE is analyzed in real circumstance,

TABLE I
PROPERTIES OF THE RT ESTIMATION METHODS

Methods	RT angles	Relationship	Searching times	Background
CRTE	All angles	–	2-D searching	No limited
ERTE	α , β	–	Two times 1-D	Ideal
CSRTE	$\pm\alpha$	$\beta=-\alpha$	Two times 1-D	Clutter
NBRTE	α , β	–	Two times 1-D	Noise
ALRTE	α , β , $\tilde{\beta}$	$\tilde{\beta}=2\hat{\theta}-\alpha$	Three times 1-D	Optimal angles
URRTE	$\pm\alpha$, $\pm\tilde{\beta}$	$\tilde{\beta}=2\hat{\theta}-\alpha$	Four times 1-D	No limited

and the robust methods are proposed by exploiting the geometry information furthermore. For illustrative purposes, the properties of the proposed methods and the CRTE method are compared in Table I in advance.

A. CSRTE in the RT Domain

Since the fast moving target spectrum is shifted from the main clutter spectrum, the fast moving target surrounding background possesses much higher signal-to-clutter ratio (SCR), which is analyzed in this part. Given the measurement procedure of the LNPs, we realize that the higher the SCR is, the more accurate the LNPs achieve. Different from the existing clutter suppression methods, the CSRTE method is proposed to cancel clutter in the RT domain. Moreover, much more geometry information of the clutter cancellation results is exploited in the RT domain to make it compatible with the proposed ERTE method, and then, the radial velocity of the moving target can be estimated.

1) Clutter Cancellation in the RT Domain: We present the clutter cancelling approach first to reduce the clutter contamination. As is known, the radial velocity of the clutter is zero, so the stationary targets can be used to represent the clutter. Thus, the clutter is mathematically expressed by

$$c(\tau,\eta)=\sum_{n=1}^{N}\sigma_{cn}A\cdot\operatorname{sinc}\left[B_r\left(\tau-\frac{2R_n}{c}\right)\right]\cdot\operatorname{rect}\left[\frac{\eta}{T_a}\right]\exp\left[-\frac{j4\pi f_c}{c}\left(R_n+\frac{v^2}{2R_n}\eta^2\right)\right] \quad (13)$$

where the number of stationary targets is set as N at most and σ_{cn} and R_n denote the complex reflection coefficient and the nearest slant range of the nth stationary target, respectively. The $\pm\alpha$-RTs of the clutter can be derived by (5) and (13) as

$$C_R(\rho,\alpha)=\sum_{\eta=-\frac{T_a}{2}}^{\eta=+\frac{T_a}{2}}\sum_{n=1}^{n=N}\sum_{\tau=\frac{2R_n}{c}-\frac{T_p}{2}}^{\tau=\frac{2R_n}{c}+\frac{T_p}{2}}\delta\left(\rho-\tau\cos\alpha-\eta\sin\alpha\right)\cdot\left|\sigma_{cn}A\cdot\operatorname{sinc}\left[B_r(\tau-2R_n/c)\right]\right| \quad (14)$$

$$C_R(\rho,-\alpha)=\sum_{\eta=-\frac{T_a}{2}}^{\eta=+\frac{T_a}{2}}\sum_{n=1}^{n=N}\sum_{\tau=\frac{2R_n}{c}-\frac{T_p}{2}}^{\tau=\frac{2R_n}{c}+\frac{T_p}{2}}\delta(\rho-\tau\cos\alpha+\eta\sin\alpha)\cdot\left|\sigma_{cn}A\cdot\operatorname{sinc}\left[B_r(\tau-2R_n/c)\right]\right|. \quad (15)$$

The trajectory of the clutter, which is perpendicular without range walk, is symmetrical about $\eta=0$ in the range compression domain, so (15) can be rewritten as

$$C_R(\rho,-\alpha)=\sum_{\eta=-\frac{T_a}{2}}^{\eta=+\frac{T_a}{2}}\sum_{n=1}^{n=N}\sum_{\tau=\frac{2R_n}{c}-\frac{T_p}{2}}^{\tau=\frac{2R_n}{c}+\frac{T_p}{2}}\delta(\rho-\tau\cos\alpha-\eta\sin\alpha)\cdot\left|\sigma_{cn}A\cdot\operatorname{sinc}\left[B_r(\tau-2R_n/c)\right]\right|. \quad (16)$$

Comparing (14) with (16), we can find that the $\pm\alpha$-RTs of the clutter keep the same as each other, i.e., $C_R(\rho,\alpha)=C_R(\rho,-\alpha)$.

On the other hand, the $\pm\alpha$-RTs of the moving target can be derived by (2) and (5) as

$$S_R(\rho,\alpha)=\sum_{\eta=-\frac{T_a}{2}}^{\eta=+\frac{T_a}{2}}\sum_{\tau=\frac{2R_0}{c}-\frac{T_p}{2}}^{\tau=\frac{2R_0}{c}+\frac{T_p}{2}}\delta(\rho-\tau\cos\alpha-\eta\sin\alpha)\cdot\left|\sigma_sA\cdot\operatorname{sinc}\left[B_r\left(\tau-2(R_0+v_r\eta)/c\right)\right]\right| \quad (17)$$

$$S_R(\rho,-\alpha)=\sum_{\eta=-\frac{T_a}{2}}^{\eta=+\frac{T_a}{2}}\sum_{\tau=\frac{2R_0}{c}-\frac{T_p}{2}}^{\tau=\frac{2R_0}{c}+\frac{T_p}{2}}\delta(\rho-\tau\cos\alpha+\eta\sin\alpha)\cdot\left|\sigma_sA\cdot\operatorname{sinc}\left[B_r\left(\tau-2(R_0+v_r\eta)/c\right)\right]\right|. \quad (18)$$

Because of the range walk in the range compression domain, the $\pm\alpha$-RTs of the moving target are different from each other, i.e., $S_R(\rho,\alpha)\neq S_R(\rho,-\alpha)$.

These properties of the moving target and clutter in the symmetry angle RT domain $S_R(\rho,\alpha)\neq S_R(\rho,-\alpha)$ and $C_R(\rho,\alpha)=C_R(\rho,-\alpha)$ can be demonstrated by the following simulated results visually.

In Fig. 6(a) and (b), the moving target with a radial velocity of 30 m/s, the clutter with a radial velocity of zero, and their combination are transformed by α- and $-\alpha$-RTs, where P_s^{α}, P_c^{α}, P_{sc}^{α}, $P_s^{-\alpha}$, $P_c^{-\alpha}$, and $P_{sc}^{-\alpha}$ denote the corresponding projections, respectively. It can be seen that P_s^{α} and $P_s^{-\alpha}$ are different from each other in LNP and amplitude, and the similar case occurs for P_{sc}^{α} and $P_{sc}^{-\alpha}$, while P_c^{α} keeps the same as $P_c^{-\alpha}$. Thus, the simulation results demonstrate the derived properties of the moving target and clutter in the RT domain. These two important properties $S_R(\rho,\alpha)\neq S_R(\rho,-\alpha)$ and $C_R(\rho,\alpha)=C_R(\rho,-\alpha)$ state different geometries in the RT domain. Conscious of these, we utilize the subtraction between the α-RT and $-\alpha$-RT results to cancel the clutter but reserve the moving target in the RT domain.

As shown in Fig. 6(c), P_c, P_s, and P_{sc} denote the cancelled results of the $\pm\alpha$-RTs, i.e., $P_c=P_c^{\alpha}-P_c^{-\alpha}$, $P_s=P_s^{\alpha}-P_s^{-\alpha}$, and $P_{sc}=P_{sc}^{\alpha}-P_{sc}^{-\alpha}$. It can be seen from Fig. 6(c) that the cancelled results of clutter P_c is almost zero because of $C_R(\rho,\alpha)=C_R(\rho,-\alpha)$ while that of moving target P_s and the combination P_{sc} are reserved due to $S_R(\rho,\alpha)\neq S_R(\rho,-\alpha)$. Thus, the clutter cancellation in the RT domain is feasible. However, it should be noted that the cancellation approach would become ineffective as the range walk angle θ of the moving target approaches to 0°. The cancellation performance degrading caused by small θ is analyzed to given the effective scope of the CSRTE method. If the LNPs can be identified from each other in the $\pm\alpha$-RT domain (i.e., $|L_{\alpha}-L_{-\alpha}|>1$), the clutter

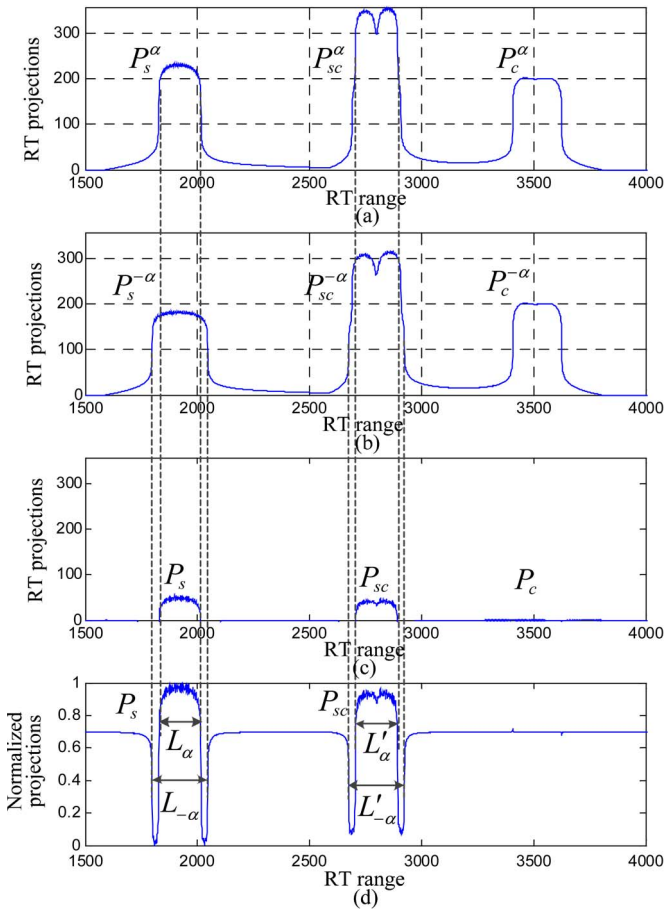

Fig. 6. Sketch of the CSRTE method. (a) and (b) $\pm\alpha$-RT results. (c) Clutter cancellation results. (d) Normalized clutter cancellation results.

cancellation performance would not degrade. Given (9) and (10), we can obtain the following symbolical representation:

$$\begin{aligned} |L_\alpha - L_{-\alpha}| &= |L_\theta \sin(\alpha-\theta) - L_\theta \sin(\theta+\alpha)| \\ &= |L_\theta \cdot 2\cos\alpha \sin\theta| \\ &= \left| \left(\frac{T_a f_{sa}}{\cos\theta} \right) \cdot 2\cos\alpha \sin\theta \right| \\ &= |2T_a f_{sa} \cos\alpha \tan\theta| > 1. \end{aligned} \tag{19}$$

Then, the effective scope of the range walk angles restricted by the clutter cancellation in the $\pm\alpha$-RT domain can be derived by (19) as

$$|\tan\theta|_{\min}^{\alpha-\mathrm{CSRTE}} > \frac{1}{(2T_a f_{sa}|\cos\alpha|)}. \tag{20}$$

It can be seen from (20) that $|\tan\theta|_{\min}^{\alpha-\mathrm{CSRTE}}$ is affected by not only the synthetic aperture time and PRF but also the RT angle α. Given $|\tan\theta|_{\min}^{\mathrm{RT}}$ in (7), we can find that

$$\begin{aligned} |\tan\theta|_{\min}^{\mathrm{RT}} &= \frac{f_{sr}}{B_r f_{sa} T_a} > \frac{1}{f_{sa} T_a} > \frac{1}{(2T_a f_{sa}|\cos\alpha|)} \\ &= |\tan\theta|_{\min}^{\alpha-\mathrm{CSRTE}}, |\cos\alpha| > 0.5. \end{aligned} \tag{21}$$

It is noteworthy that the condition of $|\cos\alpha| > 0.5$ can be satisfied easily by selecting an appropriate α, and then, $|\tan\theta|_{\min}^{\mathrm{RT}} > |\tan\theta|_{\min}^{\alpha-\mathrm{CSRTE}}$ is obtained. This analysis provides evidence that the effective scope caused by CSRTE is much looser than that due to the RT-based estimation method. In other words, the clutter cancellation performance would not degrade in the RT-based estimation method.

2) Radial Velocity Estimation: After clutter cancellation in the RT domain, the LNPs of the $\pm\alpha$-RTs should be measured to estimate the radial velocity of the moving target accordingly. As shown in Fig. 6(d), superficially, it is hard to find the relationship between $\pm\alpha$-RTs of the moving target and the corresponding LNPs in the cancelling results. Therefore, much more underlying geometry information should be exploited to obtain the LNPs L_α and $L_{-\alpha}$.

It can be seen from Fig. 6(d) that the cancelled projections possess not only protruding but also depressed parts. Let us take the results of the moving target, for example, to explain the reason. In the cancelling procedure, the higher projection P_s^{α} in amplitude subtracts with the lower one $P_s^{-\alpha}$, leading to protruding results, and the narrower projection P_s^{α} in LNP subtracts with the wider one $P_s^{-\alpha}$, resulting in the depressed parts. Consequently, the lengths of the protruding and depressed parts correspond to the LNPs of α-RT and $-\alpha$-RT, respectively, shown by the dashed lines from Fig. 6(a) to Fig. 6(d). The same corresponding relationship is still valid for the combination of the moving target and clutter, since the clutter has been cancelled.

The LNPs of $\pm\alpha$-RTs of the moving target and the combination are measured as L_α, $L_{-\alpha}$, L'_α, and $L'_{-\alpha}$, as shown in Fig. 6(d). Then, the radial velocity of the moving target can be estimated by (12) in clutter background as

$$\hat{v}_{r,\mathrm{CSRTE}} = \frac{c f_{sa} \tan\alpha}{2 f_{sr}} \frac{L'_{-\alpha} - L'_\alpha}{L'_{-\alpha} + L'_\alpha}. \tag{22}$$

The estimation of (22) is derived by (12) and $\beta = -\alpha$, so the estimation of (22) can effectively estimate the radial velocity of moving targets as long as (20) is satisfied. Given the relationship of (21), we can conclude that (22) is effective in estimating the radial velocity provided that the radial velocity can be estimated by the RT-based method. To evaluate the estimation performance degrading due to the clutter cancelling procedure, radial velocity estimation by L'_α and $L'_{-\alpha}$ is compared with that by L_α and $L_{-\alpha}$. Moreover, the estimation results keep the same as 30.2215 m/s; in other words, the estimated radial velocity is not affected by the clutter cancelling procedure. Thus, the CSRTE method can be used to estimate the radial velocity of moving targets in clutter background.

B. NBRTE

In Gaussian noise background, the CRTE method enhances the signal-to-noise ratio (SNR) in the RT domain by angle searching, and the best matched angle corresponds to the highest energy of the RT results. However, it is impractical for the proposed ERTE because of only two angles involved. In order to apply the proposed method in noise background, we should solve the problem on how to improve the SNR of the RT results by only two angles for accurate estimation. In this section, we present the NBRTE method, by exploiting the different geometry properties of noise and moving target in the RT domain, to estimate the radial velocity in the noise background.

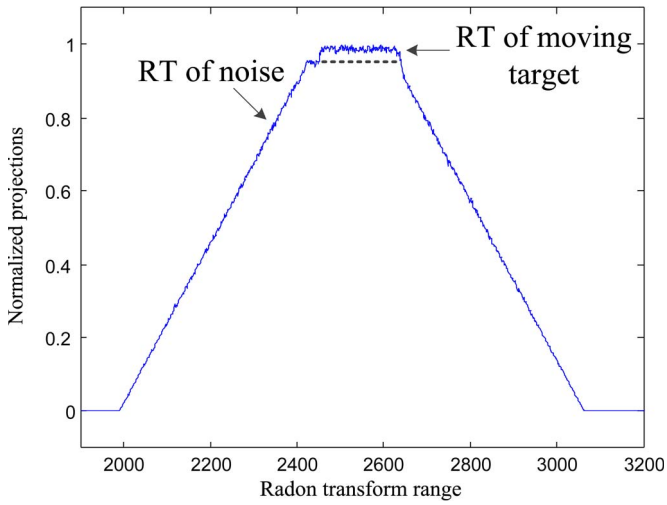

Fig. 7. 5°-RT of moving targets in the noise background.

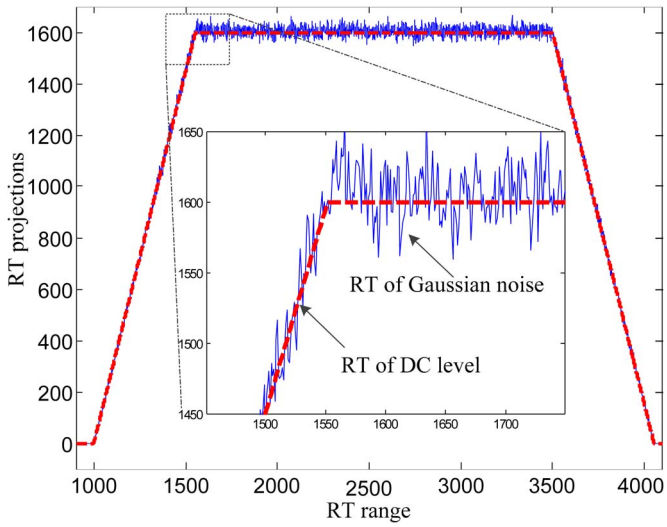

Fig. 8. RTs of Gaussian noise and constant value.

As mentioned earlier, the range walk angles of ground moving targets can be located into the interval of $[-5^\circ, 5^\circ]$, and the moving target energy increases as $|\theta + (90^\circ - \varphi)|$ approaches to 90°. Thus, the two angles α and β for RTs should be selected as $\pm 5^\circ$, respectively, to obtain as high SNR in the RT domain as possible.

In the noise background with an SNR of 18 dB in the range compression domain, a moving target with a radial velocity of 30 m/s is simulated, with its normalized projections of the 5°-RT shown in Fig. 7. Different from the ideal case in Fig. 2(c), the shape of the normalized projections in the noise background is approximately a trapezoid, where the moving target is hard to be separated from. The reason for the approximate trapezoid-shaped normalized projections is explained as follows. As is known, the absolute operation in (5) brings direct current (dc) level and random amplitude of noise. Moreover, the RT of the same value in the 2-D plane would bring rigorous trapezoid-shaped projection. Consequently, the dc level leads to the trapezoid-shaped RT results, while the random amplitude leads to a tiny random edge of the normalized projection.

Given the mechanism of the trapezoid-shaped RT results, we compare the RTs of Gaussian noise with that of its dc level. As shown in Fig. 8, the shapes of the two RTs keep the same, while the edges of the two RTs are slightly different from each other. In contrast, this phenomenon would not occur for the moving target because the trajectory of the moving target is not entire but local in the 2-D range compression domain. Thus, the RT of the dc level of the noise background can be used to cancel the trapezoid-shaped RT of noise but reserve the moving target in the RT domain, as shown in Fig. 9.

After the noise cancellation in the RT domain, the normalized projection of the moving target appears, and then, the LNP of the moving target is easy to be measured. Any two angles α and β around $\pm 5^\circ$ can be used to obtain the corresponding LNPs; afterward, the radial velocity of the moving target can be estimated by (12) as

$$\hat{v}_{r,\mathrm{NBRTE}} = \frac{cf_{sa}}{2f_{sr}} \frac{L_\beta \sin\alpha + L_\alpha \sin\beta}{L_\beta \cos\alpha + L_\alpha \cos\beta}. \tag{23}$$

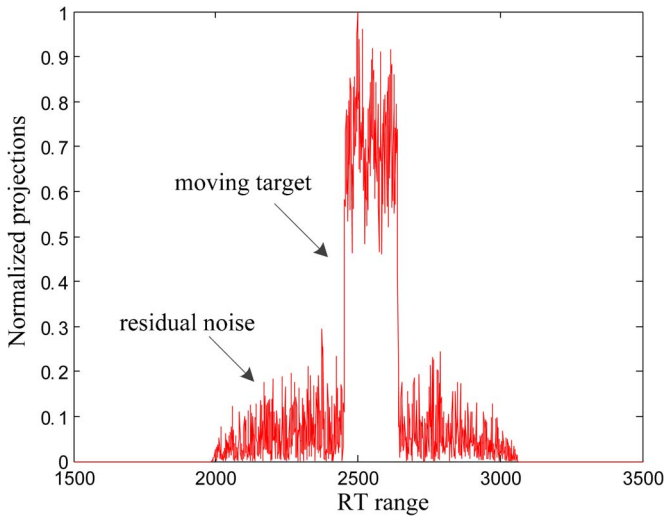

Fig. 9. Normalized projections of 5°-RT after noise cancelling in the RT domain.

C. Minimize the Estimation Error by ALRTE

In the aforementioned discussion, the burden of accurate estimation on threshold selection has been released by the preprocessing operation. Consequently, one can obtain the accurate estimation for the current α- and β-RTs. However, if another pair of α and β is used for RT, much more accurate estimation results may be obtained. In this section, the optimal angle pair for the fixed threshold is learned by utilizing the geometry information to obtain a much more accurate estimation.

For simplicity, it is assumed that the measured errors of the LNPs by a fixed threshold keep the same as ΔL for any pair of RT angles. Then, the radial velocity estimation by the LNPs with measured errors can be rewritten as

$$\hat{v}_r' = \frac{cf_{sa}}{2f_{sr}} \frac{(L_\beta + \Delta L)\sin\alpha + (L_\alpha + \Delta L)\sin\beta}{(L_\beta + \Delta L)\cos\alpha + (L_\alpha + \Delta L)\cos\beta}. \tag{24}$$

Subsequently, the estimated error of the radial velocity can be derived by (24) as (25), shown at the top of the next page.

$$|\Delta\hat{v}_r| = \frac{cf_{sa}}{2f_{sr}}\left|\frac{L_\beta\sin\alpha + L_\alpha\sin\beta}{L_\beta\cos\alpha + L_\alpha\cos\beta} - \frac{(L_\beta+\Delta L)\sin\alpha + (L_\alpha+\Delta L)\sin\beta}{(L_\beta+\Delta L)\cos\alpha + (L_\alpha+\Delta L)\cos\beta}\right|$$
$$= \frac{cf_{sa}}{2f_{sr}}\frac{|\sin(\alpha-\beta)(L_\beta-L_\alpha)\Delta L|}{(L_\beta\cos\alpha + L_\alpha\cos\beta)\left((L_\beta+\Delta L)\cos\alpha + (L_\alpha+\Delta L)\cos\beta\right)} \tag{25}$$

Regardless of $|\sin(\alpha-\beta)| = 0$ and $\Delta L = 0$, the minimum estimated error can be obtained when

$$L_\alpha = L_\beta. \tag{26}$$

According to the geometric relationship of (9) and (10), the condition of (26) can be satisfied if

$$\tilde{\beta} = 2\hat{\theta} - \alpha \tag{27}$$

where $\hat{\theta}$ is the estimated range walk angle of the moving target by the initial pair of α and β, and $\tilde{\beta}$ is an extra RT angle for much more accurate estimation. Then, the radial velocity can be estimated by

$$\hat{v}_{r,\mathrm{ALRTE}} = \frac{cf_{sa}}{2f_{sr}}\frac{L_{\tilde{\beta}}\sin\alpha + L_\alpha\sin\tilde{\beta}}{L_{\tilde{\beta}}\cos\alpha + L_\alpha\cos\tilde{\beta}}. \tag{28}$$

Thus, the ALRTE method with angle learning via (27) can be implemented by three times 1-D searching operation to minimize the estimation error due to angle selection. Although an extra RT is used, the estimation accuracy is improved effectively, which would be validated by the simulations in Section V.

D. Comprehensive Consideration by a URRTE

In the three aforementioned sections, clutter, noise, and estimation error due to angle selection are analyzed, and their corresponding robust methods are presented independently. In this section, the three robust methods are unified together as URRTE to possess all of their advantages.

Comparison among the three aforementioned methods is shown as Table I. It is noteworthy that the NBRTE method can be combined with CSRTE or ALRTE easily, while the CSRTE method keeps inconsistent with ALRTE. In the CSRTE method, the $\pm\alpha$-RTs are used to cancel clutter and obtain the estimated range walk angle $\hat{\theta}$, while in the ALRTE method, the α-RT and β-RT are utilized to obtain a primary estimation, and $\tilde{\beta}$-RT is used to minimize the estimated error. The CSRTE can be modified to reconcile with the ALRTE by once more CSRTE with $\pm\tilde{\beta}$-RTs, where $\tilde{\beta}$ is learned by the initial α and the estimated range walk angle $\hat{\theta}$. Consequently, the procedure of the URRTE method is given as follows.

Step 1) Initialize the RT angles as $\pm\alpha$, and compute the $\pm\alpha$-RTs of the trajectory of the moving target in the range compression domain.

Step 2) Cancel the clutter in the RT domain by $\pm\alpha$-RT subtraction, and cancel noise in the RT domain by the RTs of the dc level of noise.

Step 3) Measure the LNPs of the moving target in the RT domain as L_α and $L_{-\alpha}$ by a normalized threshold.

Step 4) Calculate the range walk angle by $\hat{\theta} = \mathrm{atan}(\tan\alpha \cdot (L_{-\alpha} - L_\alpha)/(L_{-\alpha} + L_\alpha))$.

Step 5) Learn extra RT angle by $\tilde{\beta} = 2\hat{\theta} - \alpha$, and compute the $\pm\tilde{\beta}$-RTs of the trajectory of the moving target in the range compression domain.

Step 6) Cancel the clutter in the RT domain by $\pm\tilde{\beta}$-RT subtraction, and cancel noise in the RT domain by the RTs of the dc level of noise.

Step 7) Measure the LNPs of the moving target in the RT domain as $L_{\tilde{\beta}}$ and $L_{-\tilde{\beta}}$ by the same normalized threshold.

Step 8) By utilizing the LNPs of L_α and $L_{\tilde{\beta}}$, the best matched angle $\hat{\theta}_{\mathrm{opt}}$ can be calculated via

$$\hat{\theta}_{\mathrm{opt}} = \mathrm{atan}\left[\frac{\left(L_{\tilde{\beta}}\sin\alpha + L_\alpha\sin\tilde{\beta}\right)}{\left(L_{\tilde{\beta}}\cos\alpha + L_\alpha\cos\tilde{\beta}\right)}\right]$$

and the radial velocity is obtained by

$$\hat{v}_{r,\mathrm{URRTE}} = \frac{cf_{sa}\left(L_{\tilde{\beta}}\sin\alpha + L_\alpha\sin\tilde{\beta}\right)}{2f_{sr}\left(L_{\tilde{\beta}}\cos\alpha + L_\alpha\cos\tilde{\beta}\right)}.$$

Since four times RTs are used to estimate the accurate radial velocity in real circumstance, the URRTE method requires four times 1-D searching operation. In the procedure of the URRTE method, the CSRTE is contained in steps 1, 2, 3, 6, and 7 to cancel clutter, the NBRTE is expressed by steps 2 and 6 to cancel noise, and the ALRTE is reflected by step 5 to minimize the estimation error. Thus, containing three robust methods, the URRTE possesses the advantages of the three methods, which would achieve much more accurate estimation in real circumstance than the others. These theoretical analyses would be validated by the following experimental results.

V. Experimental Results and Analysis

Simulation and real data process are given to verify the theoretical conclusion of the proposed methods. The system parameters are shown in Table II. It can be seen that the range and azimuth are oversampled, and there may exist several best matched range walk angles. By averaging the estimated results, the estimation accuracy would not be degraded seriously.

A. Comparison With the CRTE

A computationally attractive comparison between the ERTE and CRTE is simulated in the clutter-free background. Given the aforementioned shortcomings of the CRTE method, we

TABLE II
SYSTEM PARAMETERS

Parameters	symbols	values
Carrier frequency/GHz	f_c	8.85
Band width/MHz	B	40
Sampling frequency/MHz	f_{sr}	60
Velocity of the platform/(m/s)	v	120
Pulse repetition frequency/Hz	f_{sa}	1000
Two-way azimuth beam width/rad	θ_{bw}	0.0085
Nearest slant-range/m	R_0	9000

TABLE III
COMPARISON BETWEEN THE ERTE AND CRTE METHODS

Radial velocities (m/s)		30.0000	40.0000	50.0000	60.0000
Estimation results (m/s)	CRTE1	30.5448	39.2731	50.1850	61.0987
	CRTE2	29.8902	39.9278	49.9667	60.2255
	ERTE	30.2835	40.1840	50.1429	59.7948
Computing time (s)	CRTE1	60.2985	59.2226	59.3893	59.9079
	CRTE2	550.4187	545.2467	543.7691	542.8613
	ERTE	0.1493	0.1346	0.1311	0.1331

utilize two CRTEs with different angle searching step sizes of 0.05° (CRTE1) and 0.005° (CRTE2) to estimate the radial velocities of moving targets, together with the angle searching range of $[-5°, 5°]$. Without loss of generality, several radial velocities are estimated, with the estimation results shown in Table III.

From Table III, we can see that the CRTE2 possesses the highest estimation accuracy with the hugest computing time of 545.5739 s in average, while the ERTE realizes the comparable estimation accuracy with the CRTE2 by using the least computing time of only 0.1370 s averagely, and the worst estimation results are obtained by the CRTE1 also with the huge computing time of 59.7046 s in average. The accurate estimation and low computation load advantages of the proposed ERTE are validated effectively by these comparisons, which provides evidence that the proposed ERTE method behaves much better than the CRTE method, especially for the real-time estimation.

B. Clutter Background Simulation and Comparison Analysis

The estimation performances among the CRTE (with a searching step size of 0.05°), CSRTE, and URRTE are compared in different SCR (SCR $\in [0$ dB, 20 dB$]$) backgrounds. The relative errors of the estimated radial velocity are shown in Fig. 10.

It can be seen that the URRTE behaves better than the CSRTE in all SCRs, which becomes much more obvious as the SCR increases. This is because the URRTE method can cancel clutter and minimum estimation error simultaneously, while the CSRTE method is only capable of clutter cancellation. Moreover, the estimation accuracy is affected mainly by the clutter, on the one hand, in the low SCR scenario but the estimation error due to angle selection, on the other hand, in the high SCR case. Therefore, the URRTE method performs much better than the CSRTE in the same clutter background, which verifies the aforementioned theoretical conclusion.

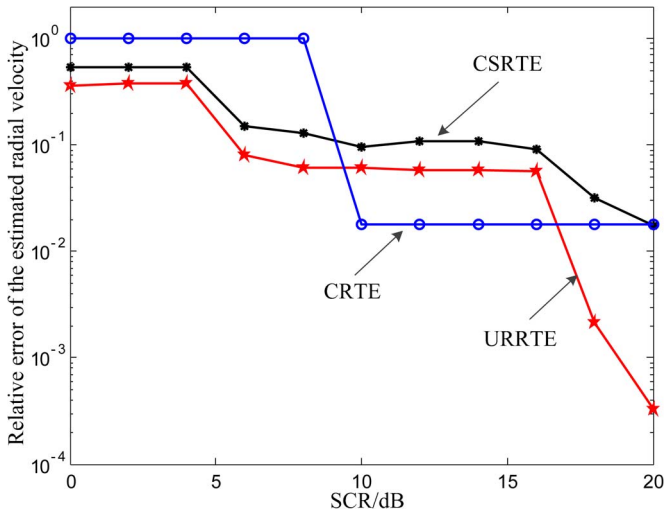

Fig. 10. Comparison in different SCR clutter backgrounds.

Furthermore, the estimated relative error by the CRTE method is only two levels as the SCR increases in Fig. 10. The estimated values are used to explain the reason. When the SCR is lower than 10 dB, all of the estimated results by the CRTE are 0 m/s, which correspond to the radial velocity of clutter. Consequently, when the SCR is lower than 10 dB, the energy of the clutter is much higher than that of the moving target in the RT domain, and then, the estimated results keep the same. On the other hand, provided that the energy of the moving target is higher than that of the clutter, the estimation results by the CRTE would be the radial velocity of the moving target, which also keeps unchanged as the SCR increases. Moreover, in the SCR range of [10 dB, 16 dB], the estimation accuracy by the CRTE is better than that by the CSRTE and URRTE. This is because the estimation accuracy improvement by clutter cancellation in the RT domain (CSRTE and URRTE) is not better than that by angle searching (CRTE). As the SCR increases, the estimation by the CSRTE and URRTE becomes much more accurate, and the competitive advantage of the URRTE on estimation accuracy appears.

C. Noise Background Simulation and Comparison Analysis

Radial velocity estimation comparison among the CRTE (with a searching step size of 0.05°), ERTE, NBRTE, and URRTE methods is simulated in noise background with different SNRs of the range compression results. The comparison results via 100 times Monte Carlo experiments are shown in Fig. 11.

Compared with the CRTE, the NBRTE and URRTE possess much more accurate estimation in high SNR case of SNR $>$ 20 dB, but the ERTE becomes better than CRTE when SNR $>$ 38 dB. Given the theoretical analysis and the experimental results, we can get the following four conclusions. First, the estimation accuracy of the CRTE is limited by the angle searching step size, but the proposed methods (ERTE, NBRTE,

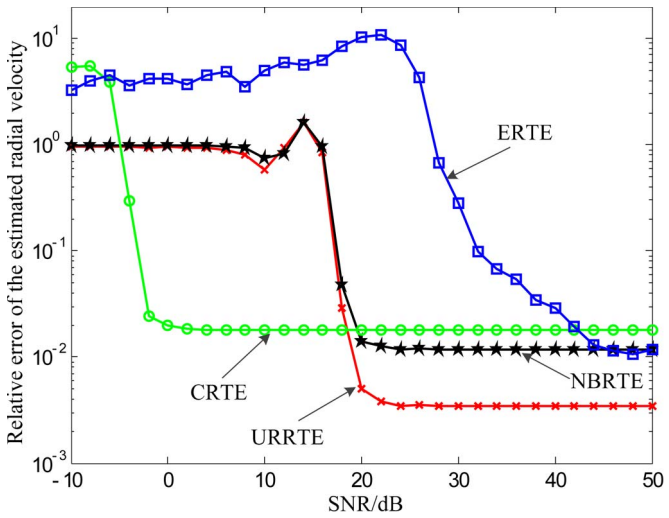

Fig. 11. Comparison in different SNR noise backgrounds.

and URRTE) can break through the estimation accuracy limit and realize much higher estimation accuracy in high SNR background. Second, the estimation accuracy improvements by noise cancellation (NBRTE) and RT angle optimization (URRTE) are better than that by angle searching (CRTE) when SNR $>$ 20 dB. Third, robust to noise, the NBRTE and URRTE are much more effective than the ERTE in noise background. Fourth, the estimation accuracy by the URRTE is much higher than that by the NBRTE in all SNRs, which is more obvious when SNR $>$ 20 dB, with similar reason to the clutter background.

D. Real Data Process

Recorded by an airborne X-band radar system with parameter list in Table II, real data are processed to demonstrate the validity of the proposed methods. The aforementioned serious effect on moving target imaging due to the radial velocity is presented first, and then, the qualitative and quantitative evaluations are provided by experimental analysis utilizing the estimated radial velocity into the effectiveness of the proposed methods.

Since the moving target radial velocity estimation process is independent on the azimuth compression, the SPECAN algorithm is used to generate the image, as shown in Fig. 12. The azimuth resolution of the SPECAN algorithm can be calculated by $\rho_a = 0.886\ \mu_w v/B_a \approx 2.4$ m, where the Doppler bandwidth B_a can be calculated by $B_a = |K_a|T_a = (2v^2/\lambda R_0) \times (R_0\theta_{bw}/v) = 60.3216$ Hz and μ_w is the spanning factor as 1.36 due to the azimuth window. It can be seen from Fig. 12 that the moving targets are submerged in the strong clutter. The clutter suppression results by the extended factored approach [28], [29] are shown as Fig. 13, where the moving targets can be detected easily. However, because of the radial velocity, the moving targets are displaced from the road where they should be.

The range walk of the fast moving target is shown as Fig. 14, where the range gate of the moving target area has been redefined to obviously represent the range walk of the fast moving target. The CRTE and URRTE methods are used to estimate the radial velocity of the fast moving target, with the

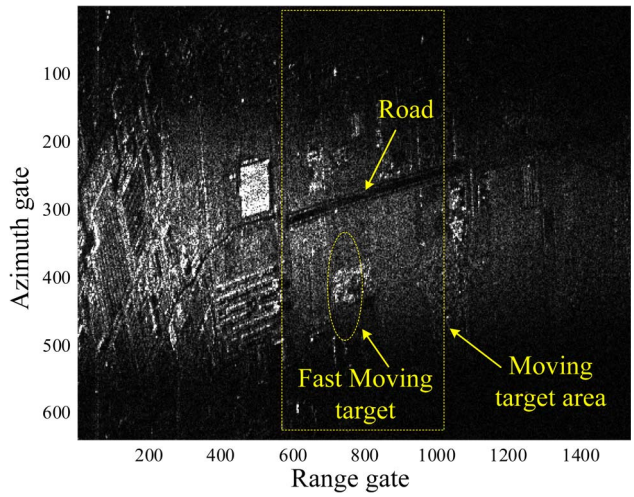

Fig. 12. SAR image of the scene.

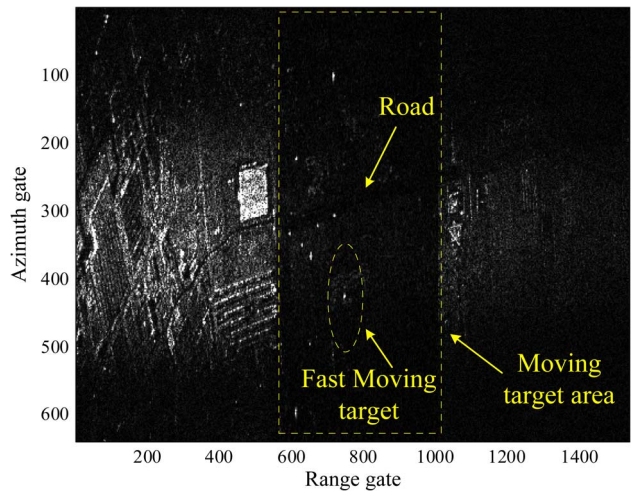

Fig. 13. SAR image of the scene after clutter suppression of moving target area.

estimated results of $\hat{v}_{r,\mathrm{URRTE}} = 20.6790$ m/s and $\hat{v}_{r,\mathrm{CRTE}} = 22.0768$ m/s, respectively. To validate the URRTE method, the estimated radial velocity $\hat{v}_{r,\mathrm{URRTE}}$ is used to correct the range walk, with the correction results shown in Fig. 15.

Compared with the prior results in Fig. 14, the range walk of the fast moving target is well corrected by $\hat{v}_{r,\mathrm{URRTE}}$. The qualitative assessment has been validated by the range walk correction, and the quantitative analysis would be provided by the moving target localization in azimuth.

As is known, the azimuth displacement ΔX of the moving target due to its radial velocity can be given by

$$\Delta X = \mathrm{round}\left(\frac{R_m \tilde{v}_r}{\rho_a v}\right) \tag{29}$$

where round$(\cdot)$ is the rounding operation, R_m is the range gate of the moving target locating, ρ_a is the azimuth resolution as 2.4 m, and $\tilde{v}_r$ is the ambiguous estimated radial velocity of the fast moving target, which can be calculated by the Doppler ambiguity and the estimated radial velocity $\hat{v}_r$ as $\tilde{v}_r = \mathrm{mod}(2f_c\hat{v}_r/c, PRF) \cdot c/2f_c$, where $\mathrm{mod}(a, b)$ is the modulus of a/b. Then, the azimuth displacement of the fast moving

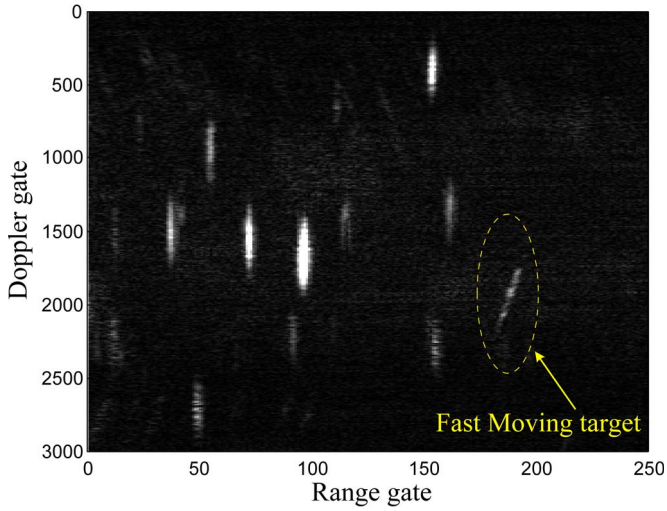

Fig. 14. Range walk of moving targets after clutter suppression.

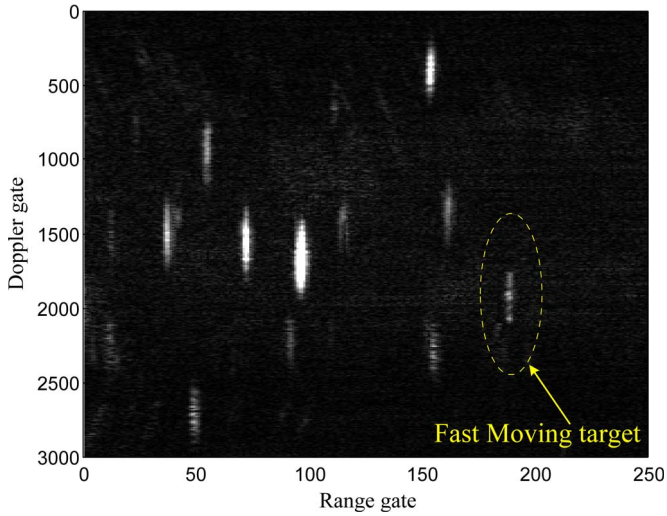

Fig. 15. Range walk correction result of the fast moving target.

target can be calculated by (29) and $\hat{v}_{r,\mathrm{URRTE}}$ as $\Delta X_{\mathrm{URRTE}} = 148$ m, while that by $\hat{v}_{r,\mathrm{CRTE}}$ is $\Delta X_{\mathrm{CRTE}} = 105$ m. The relocation results are shown in Fig. 16. It is noteworthy that the fast moving target is accurately relocated in the original road by the estimated radial velocity of $\hat{v}_{r,\mathrm{URRTE}}$, which demonstrates the effectiveness of the proposed method quantitatively.

With high estimation accuracy and low computation complexity, the URRTE is more efficient to estimate the radial velocity of moving targets in real circumstance. Furthermore, the moving target can be also relocated with high accuracy, even when the ambiguity occurs.

VI. Conclusion

This paper primarily has presented an ERTE and its robust forms for radial velocity of moving target. By utilizing the geometry information, the proposed methods can calculate rather than search for the radial velocity of moving targets, which simplifies the conventional 2-D searching operation into only two to four times 1-D searching operation. Furthermore, by exploiting the geometry information in the RT domain, the

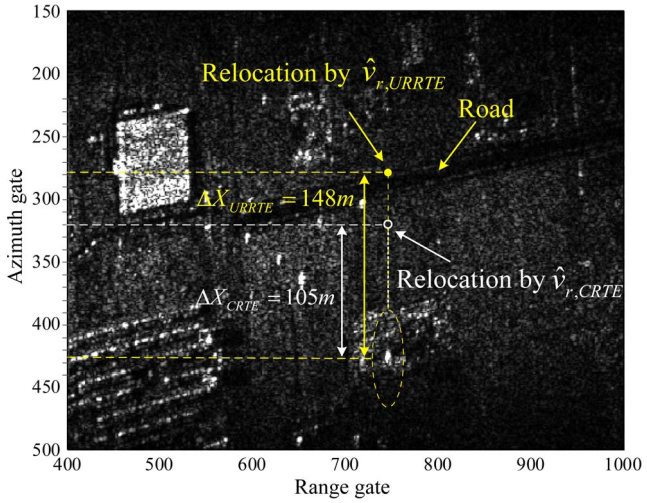

Fig. 16. Relocation results of the fast moving target.

three robust methods are capable of clutter cancellation, noise cancellation, and estimation error minimizing, respectively. Moreover, the unified robust method possesses much more accurate estimation than the other proposed methods, which can be used in real circumstance. Theoretical and experimental analysis provides qualitative and quantitative evaluations into the effectiveness of the proposed methods.

The key contribution of this paper is the presentation of the ERTE for radial velocity by utilizing the geometry information, to reduce the heavy computation load of the conventional method in great extent. Moreover, the potential geometry information in the RT domain is exploited as much as possible to apply the proposed methods in real circumstance. The proposed methods can be used for accurate radial velocity estimation in the single-channel SAR system, especially for real-time estimation with high-SCNR scenarios. Further investigations will be focused on the efficient motion parameter estimation for multiple moving targets.

Acknowledgment

The authors would like to thank the anonymous reviewers for their valuable and useful comments and suggestions which helped in improving this paper.

References

[1] S. Q. Zhu, G. S. Liao, H. H. Tao, Y. Qu, and Z. W. Yang, "Ground moving target detection and velocity estimation based on spatial multilook processing for multichannel airborne SAR," *IEEE Trans. Aerosp. Electron. Syst.*, vol. 49, no. 2, pp. 1322–1337, Apr. 2013.

[2] C. H. Gierull, I. Sikaneta, and D. Cerutti-Maori, "Two-step detector for RADARSAT-2's experimental GMTI mode," *IEEE Trans. Geosci. Remote Sens.*, vol. 51, no. 1, pp. 436–454, Jan. 2013.

[3] B. Deng, X. Li, H. Q. Wang, Y. L. Qin, and J. T. Wang, "Fast raw-signal simulation of extended scenes for missile-borne SAR with constant acceleration," *IEEE Geosci. Remote Sens. Lett.*, vol. 8, no. 1, pp. 44–48, Jan. 2011.

[4] G. C. Sun, M. D. Xing, X. G. Xia, Y. R. Wu, and Z. Bao, "Robust ground moving-target imaging using deramp-keystone processing," *IEEE Trans. Geosci. Remote Sens.*, vol. 51, no. 2, pp. 966–982, Feb. 2013.

[5] D. Cerutti-Maori, I. Sikaneta, and C. H. Gierull, "Optimum SAR GMTI processing and its application to the radar satellite RADARSAT-2 for traffic monitoring," *IEEE Trans. Geosci. Remote Sens.*, vol. 50, no. 10, pp. 3868–3881, Oct. 2012.

[6] D. Henke *et al.*, "Moving-target tracking in single-channel wide-beam SAR," *IEEE Trans. Geosci. Remote Sens.*, vol. 50, no. 11, pp. 4735–4747, Nov. 2012.
[7] S. Q. Zhu, G. S. Liao, Y. Qu, Z. G. Zhou, and X. Y. Liu, "Ground moving targets imaging algorithm for synthetic aperture radar," *IEEE Trans. Geosci. Remote Sens.*, vol. 49, no. 1, pp. 462–477, Jan. 2011.
[8] M. Arii, "Efficient motion compensation of a moving object on SAR imagery based on velocity correlation function," *IEEE Trans. Geosci. Remote Sens.*, vol. 52, no. 2, pp. 936–946, Feb. 2014.
[9] G. Li, X. Xia, J. Xu, and Y. Peng, "A velocity estimation algorithm of moving targets using single antenna SAR," *IEEE Trans. Aerosp. Electron. Syst.*, vol. 45, no. 3, pp. 1052–1062, Jul. 2009.
[10] R. Hu, B. C. Liu, T. Wang, D. Liu, and Z. Bao, "A knowledge-based target relocation method for wide-area GMTI mode," *IEEE Geosci. Remote Sens. Lett.*, vol. 11, no. 4, pp. 748–752, Apr. 2014.
[11] Y. X. Shu, G. S. Liao, and Z. W. Yang, "Robust radial velocity estimation of moving targets based on adaptive data reconstruction and subspace projection algorithm," *IEEE Geosci. Remote Sens. Lett.*, vol. 11, no. 6, pp. 1101–1105, Jun. 2014.
[12] A. Budillon, A. Evangelista, and G. Schirinzi, "GLRT detection of moving targets via multibaseline along-track interferometric SAR systems," *IEEE Geosci. Remote Sens. Lett.*, vol. 9, no. 3, pp. 348–352, May 2012.
[13] A. Budillon, V. Pascazio, and G. Schirinzi, "Estimation of radial velocity of moving targets by along-track interferometric SAR systems," *IEEE Geosci. Remote Sens. Lett.*, vol. 5, no. 3, pp. 349–353, Jul. 2008.
[14] G. Y. Wang, X. G. Xia, V. C. Chen, and R. L. Fielder, "Detection, location, imaging of fast moving targets using multifrequency antenna array SAR," *IEEE Trans. Aerosp. Electron. Syst.*, vol. 40, no. 1, pp. 345–355, Jan. 2004.
[15] G. Li, J. Xu, Y. N. Peng, and X. G. Xia, "Moving target location and imaging using dual-speed velocity SAR," *IET Radar, Sonar Navigat.*, vol. 1, no. 2, pp. 158–163, Sep. 2007.
[16] R. D. Chapman, C. M. Hawes, and M. E. Nord, "Target motion ambiguities in single-aperture synthetic aperture radar," *IEEE Trans. Aerosp. Electron. Syst.*, vol. 46, no. 1, pp. 459–468, Jan. 2010.
[17] S. Barbarossa, "Detection and imaging of moving objects with synthetic aperture radar," *IEE Proc. F Radar Signal Process.*, vol. 139, no. 2, pp. 79–88, Feb. 1992.
[18] C. Y. Chang and J. C. Curlander, "Application of the multiple PRF technique to resolve Doppler centroid estimation ambiguity for spaceborne SAR," *IEEE Trans. Geosci. Remote Sens.*, vol. 30, no. 5, pp. 941–949, Sep. 1992.
[19] P. A. C. Marques and J. M. B. Dias, "Velocity estimation of fast moving targets using a single SAR sensor," *IEEE Trans. Aerosp. Electron. Syst.*, vol. 41, no. 1, pp. 75–89, Jan. 2005.
[20] R. P. Xu, D. D. Zhang, D. H. Hu, X. L. Qiu, and C. B. Ding, "A novel motion parameter estimation algorithm of fast moving targets via single-antenna airborne SAR system," *IEEE Geosci. Remote Sens. Lett.*, vol. 9, no. 5, pp. 920–924, Sep. 2012.
[21] S. N. Madsen, "Estimating the Doppler centroid of SAR data," *IEEE Trans. Aerosp. Electron. Syst.*, vol. 25, no. 2, pp. 134–140, Sep. 1989.
[22] G. C. Sun *et al.*, "Improved ambiguity estimation using a modified fractional Radon transform," *IET Radar, Sonar Navigat.*, vol. 5, no. 4, pp. 489–495, Apr. 2011.
[23] M. Yu, J. Xu, Y. N. Peng, and X. Wang, "Joint estimation of Doppler centroid and rate for SAR with large range migration," *IET Radar, Sonar Navigat.*, vol. 1, no. 3, pp. 207–212, Jun. 2007.
[24] B. C. Liu, T. Wang, and Z. Bao, "Doppler ambiguity resolving in compressed azimuth time and range frequency domain," *IEEE Trans. Geosci. Remote Sens.*, vol. 46, no. 11, pp. 3444–3458, Nov. 2008.
[25] J. Yang, C. Liu, and Y. Wang, "Imaging and parameter estimation of fast-moving targets with single-antenna SAR," *IEEE Geosci. Remote Sens. Lett.*, vol. 11, no. 2, pp. 529–533, Feb. 2014.
[26] M. van Ginkel, C. L. Hendriks, and L. J. van Vliet, "A short introduction to the Radon and Hough transforms and how they relate to each other," Delft Univ. Technol., Delft, The Netherlands, The Quantitative Image Group Tech. Rep. Series N.QI-2004-01, pp. 1–9, 2004.
[27] S. Daming, Z. Liying, and L. Jigang, "Advanced Hough transform using a multilayer fractional Fourier method," *IEEE Trans. Image Process.*, vol. 19, no. 6, pp. 1558–1566, Jun. 2010.
[28] S. Q. Zhu, G. S. Liao, Y. Qu, X. Y. Liu, and Z. G. Zhou, "A new slant-range velocity ambiguity resolving approach of fast moving targets for SAR system," *IEEE Trans. Geosci. Remote Sens.*, vol. 48, no. 1, pp. 432–451, Jun. 2010.
[29] R. C. DiPietro, "Extended factored space-time processing for airborne radar systems," in *Proc. 26th Asilomar Conf. Signals, Syst. Comput.*, Pacific Grove, CA, USA, 1992, pp. 425–430.

Xuepan Zhang was born in Hebei, China. He received the B.S. degree in electrical engineering from Xidian University, Xi'an, China, in 2010, where he is currently working toward the Ph.D. degree in the National Laboratory of Radar Signal Processing.

His research interests include synthetic aperture radar, ground moving target indication, and motion parameter estimation.

Guisheng Liao (M'96) was born in Guiling, China. He received the B.S. degree from Guangxi University, Guangxi, China, in 1985 and the M.S. and Ph.D. degrees from Xidian University, Xi'an, China, in 1990 and 1992, respectively.

He is currently a Professor with Xidian University, where he is also the Dean of the School of Electronic Engineering. He has been a Senior Visiting Scholar with the Chinese University of Hong Kong, Shatin, Hong Kong. His research interests include synthetic aperture radar (SAR), space-time adaptive processing, SAR ground moving target indication, and distributed small satellite SAR system design.

Prof. Liao is a member of the National Outstanding Person and the Cheung Kong Scholars in China.

Shengqi Zhu (M'12) was born in Jiangxi, China, in October 1984. He received the B.S. degree in electrical engineering from Xidian University, Xi'an, China, in 2005 and the Ph.D. degree in electrical engineering from the National Laboratory of Radar Signal Processing, Xidian University, in 2010.

He is currently an Associate Professor with the National Laboratory of Radar Signal Processing, Xidian University. He has published over 50 papers in journals and conferences. He is the holder of nine granted patents in China. His current works include synthetic aperture radar (SAR), Doppler parameter estimation, space-time adaptive processing (STAP), SAR ground moving target indication (GMTI), bistatic STAP algorithms, and multiple-input–multiple-output radar and sparse array signal processing (including compressed sensing). He has also worked on systems for processing real airborne SAR data and designed the SAR/GMTI algorithms for the distributed small satellite SAR systems in China.

Dr. Zhu received the International Union of Radio Science Young Scientist Award at Istanbul, Turkey, in 2011. He was the recipient of the National Excellent Doctoral Dissertation Award nomination, the New Century Excellent Talents in University (selected by the Ministry of Education of China), and the New Scientific and Technological Star of Shaanxi Province.

Cao Zeng (M'12) was born in Suizhou, Hubei, China, in March 1979. He received the B.E. degree in electronic engineering, the M.S. degree in information and communication engineering, and the Ph.D. degree from Xidian University, Xi'an, China, in 2001, 2004, and 2008, respectively.

He is currently an Assistant Professor with the Department of Electronic Engineering, Xidian University. His research interests include array signal processing, multichannel moving target indication, and real-time system design and development of signal processing.

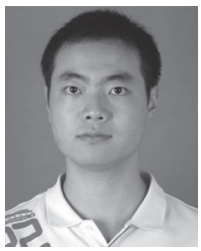

Yuxiang Shu was born in Anhui, China. He received the B.S. and Ph.D. degrees in electrical engineering from Xidian University, Xi'an, China, in 2009 and 2014, respectively.

He is currently with No.38 Research Institute, China Electronics Technology Group Corporation, Hefei, China. His research interests include synthetic aperture radar, ground moving target indication, and motion parameter estimation.